Author(s): Luukanen, A. & Kinnunen, K. M. & Nuottajärvi, A. K. & Hoevers, H. F. C. & Bergmann Tiest, W. M. & Pekola, Jukka

Title: Fluctuation-Limited Noise in a Superconducting Transition-Edge Sensor

Year: 2003

Version: Final published version

Please cite the original version:

Luukanen, A. & Kinnunen, K. M. & Nuottajärvi, A. K. & Hoevers, H. F. C. & Bergmann Tiest, W. M. & Pekola, Jukka. 2003. Fluctuation-Limited Noise in a Superconducting Transition-Edge Sensor. Physical Review Letters. Volume 90, Issue 23. 238306/1-4. ISSN 0031-9007 (printed). DOI: 10.1103/physrevlett.90.238306.

Fluctuation-Limited Noise in a Superconducting Transition-Edge Sensor

A. Luukanen, K. M. Kinnunen, and A. K. Nuottajärvi
Department of Physics, University of Jyväskylä, P.O. Box 35 (YFL) FIN-40014 University of Jyväskylä, Finland

H. F. C. Hoevers and W. M. Bergmann Tiest
SRON National Institute for Space Research, Sorbonnelaan 2, 3584 CA Utrecht, The Netherlands

J. P. Pekola
Low Temperature Laboratory, Helsinki University of Technology, P.O. Box 2200, FIN-02015 HUT, Finland
(Received 28 November 2002; published 13 June 2003)

In order to investigate the origin of the until now unaccounted excess noise and to minimize the uncontrollable phenomena at the transition in x-ray microcalorimeters we have developed superconducting transition-edge sensors into an edgeless geometry, the so-called Corbino disk, with superconducting contacts in the center and at the outer perimeter. The measured rms current noise and its spectral density can be modeled as resistance noise resulting from fluctuations near the equilibrium superconductor-normal metal boundary.

DOI: 10.1103/PhysRevLett.90.238306 PACS numbers: 85.25.Oj

At present, the most sensitive energy-dispersive x-ray detector is the transition-edge sensor (TES) microcalorimeter, a thermal detector operated typically at a bath temperature below 100 mK [1–3]. The device consists of an x-ray absorber (Bi, Au, Cu being the most common materials), thermally coupled to a TES superconducting film with a critical temperature $T_c \approx 100$ mK. The TES film is typically a proximity-coupled bilayer, e.g., Ti/Au, Mo/Cu, or Mo/Au. A common detector geometry is a square TES film, covered completely, or in some cases partially by the x-ray absorber film. The TES film-absorber combination is located on a thermally isolating Si_3N_4 film, micromachined to a bulk Si substrate which acts as the heat sink. Wires with a T_c much higher than that of the TES film are used to connect the detector to the bias circuit. The device is connected to a constant voltage bias, and the current through the sensor is measured with a superconducting quantum interference device (SQUID). The theory of operation of these devices has been well developed, but is not complete as the TES microcalorimeters consistently do not achieve the energy resolution predicted by the models. First, the TES microcalorimeters fail to reach the expected energy resolution in calorimetry, especially when the deposited heat drives the device through a large part of its superconducting transition. Second, most TESs exhibit noise in excess of the sum of the commonly recognized noise components: thermal fluctuation noise arising from the thermal link between the TES and the heat sink (TFN), Johnson noise (JN), and SQUID (readout) noise (SN). This Letter presents a simple model which explains this discrepancy in the detector subject to our study.

In the square devices, edges parallel to the current become crucial for the device performance. First, thickness variations resulting from underetching or imperfect deposition of the TES bilayer lead to spatial T_c variations. Second, the edges have also proven to give rise to flux creep noise with the higher concentration of trapping centers due to local defects which can be observable at certain values of the bias voltage. A solution to overcome edge effects is to deposit thick normal metal banks over the edges. The proximity effect of the thick normal metal reduces the critical temperature of the edges well below that of bulk of the TES film, resulting in well-defined edges [4].

Another way of removing the edges is to use a Corbino disk geometry, in which a current source is placed in the apex of the annular TES film, and another superconducting contact is placed to the outer circumference of the TES film. Here the current density is proportional to $1/r$, which results in a well-defined phase boundary at certain distance r_b from the center of the disk. A Corbino geometry TES, or the CorTES, is shown in the inset of Fig. 1. The central contact is provided by a superconducting ground plane, covering the entire sensor. By this we ensure a truly cylindrical symmetry and a homogeneous current distribution with a concentric current return.

The devices are fabricated on a double side nitridized, 525 μm thick Si wafer. Free standing Si_3N_4 membranes with a thickness of 250 nm are fabricated by wet etching of the Si. The CorTES layers are patterned by e-beam lithography, combined with UHV e-beam evaporation and lift-off. The wiring layers consist of a circular Nb outer contact, and a Nb ground plane, which contacts the TES film through an opening in an underlying insulator.

In contrast to a square TES, the phase boundary in the CorTES evolves controllably from the center of the disk and moves radially outwards with increasing current. This can be modeled by a heat transfer model, similar to that used to describe suspended Nb microbridge

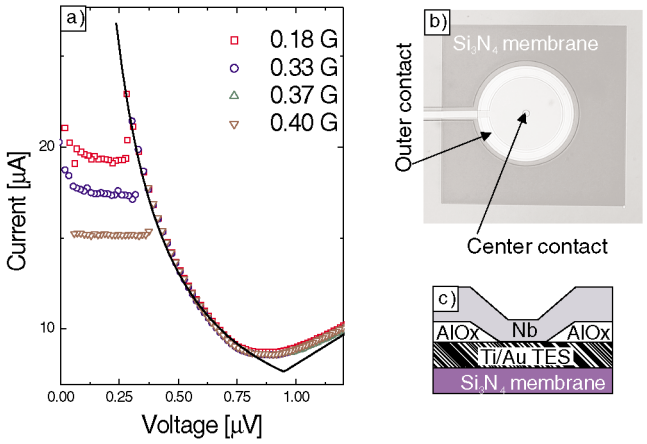

FIG. 1 (color online). (a) The measured $I(V)$ characteristics of the CorTES at different external magnetic fields denoted by the different symbols. The sensor itself is shielded by the Nb ground plane, and the $I(V)$ curve is not affected by the field. The Nb bias lines, however, are sensitive to the field and have a relatively small critical current due to difficulties in step coverage. The solid line corresponds to the fit with $\Lambda = 1.25 k_B T_c$. (b) An optical micrograph of the sensor. The radii of the center and outer contacts are 15 and 150 μm, respectively. (c) A diagram showing the layer order.

bolometers and hot electron mixers [5,6]. Assuming radial symmetry, the current density is given by $j(r) = I/(2\pi r t)$, where I is the current, r is the radial distance from the center of the disk, and t is the film thickness. Consequently, the resistance of the CorTES is given by $R = \rho_n/(2\pi t) \int_{r_0}^{r_b} 1/r dr = \rho_n/(2\pi t) \ln(r_b/r_0)$, where r_0 is the radius of the central superconducting contact. The steady-state behavior can be modeled by first noting that the heat transport within the sensor is completely dominated by the metal films. The thermal conductivity in the superconducting region (at radii $r \geq r_b$) is given approximately by $\kappa_S(T) = \kappa_N \exp[-\Lambda/k_N(1/T - 1/T_c)]$ where Λ is of the order of the energy gap Δ of the superconductor, k_B is the Boltzmann constant, $\kappa_N = LT_c/\rho_n$ is the normal state thermal conductivity, ρ_n is the normal state electrical resistivity, and $L = 2.45 \times 10^{-8}$ V^2/K^2 is the Lorentz number [7]. Here we assume validity of the Wiedemann-Franz law. The thermal conductivity of the 250 nm thick SiN membrane is given by $\kappa_M \simeq 14.5 \times 10^{-3} T^{1.98}$ [8], and at temperatures present in the system (20–150 mK) it is typically 3 orders of magnitude smaller than κ_S. As the thicknesses of the SiN and the TES are comparable, the problem reduces to two dimensions, and due to symmetry further to one dimension. At this point we neglect the temperature gradient within the normal state part, as the gradient over the superconducting annulus and especially over the surrounding membrane are much larger. In the superconducting part we require a heat balance $\dot{Q}/(2\pi t) \int_{r_b}^{r_1} 1/r\, dr = -\int_{T_c}^{T_1} \kappa_S(T)\, dT$, where $\dot{Q} = V^2 2\pi t/\rho_n \ln(r_b/r_0)$ is the dissipated bias power, with V the applied voltage across the sensor and r_1 the radius of the CorTES outer edge at temperature $T(r_1) = T_1$. A similar equation can be written for the heat transport in the membrane but now the integration is carried out from r_1 to $r_0 = 2w/\pi$, the radius of the "equivalent" circular membrane to the square one with a pitch of w, and in temperature from T_1 to T_0, the latter being the bath temperature. This leads to a solution for T_1, which can be inserted into the heat balance equation of the superconducting region. This can then be numerically solved for $r_b(V)$ from which one obtains $I(V) = V/R = 2\pi t V/\{\rho_n \ln[r_b(V)/r_0]\}$.

We first carried out an $R - T_0$ measurement in a dilution refrigerator measuring the resistance R of the CorTES using a 4-wire ac method with a current bias of 5 μA as a function of T_0. From this, $T_c = 123$ mK was obtained. Next, we measured a set current-voltage $[I(V)]$ curves using voltage bias with a source impedance R_s of 7 mΩ, and a SQUID ammeter. The results are shown in Fig. 1, together with a fit using the model above. The $I(V)$ curve is insensitive to the external magnetic field thanks to the Nb ground plane. The fitting parameter is Λ in the the superconducting region. Best fit yields $\Lambda = 1.25 k_B T_c$, which is a reasonable value, somewhat smaller than the BCS gap, $\Delta = 1.76 k_B T_c$. The sharp corner present in the fit is due to the fact that the model assumes a stepwise transition with zero width, whereas the actual transition is smooth, as seen in the inset of Fig. 2. Figure 2 shows the steepness of the transition, $\alpha = d\ln R/d\ln T$, as a function of V measured at different bath temperatures. In all the curves α has a maximum value of about 300. This is 1 order of magnitude higher than in typical (square) microcalorimeters [2]. The high α is attributed mainly to the

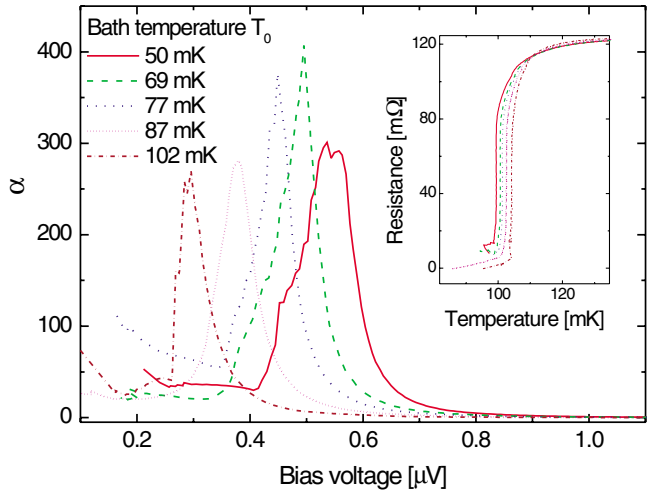

FIG. 2 (color online). Transition steepness, α, measured at different bath temperatures. A lower bath temperature corresponds to a larger bias dissipation and correspondingly larger biasing currents. However, the relative transition width remains almost unchanged. The inset shows the corresponding R-T curves calculated from the $I(V)$ curve.

self-screening property of the ground plane and the well-defined edge conditions.

The noise characteristics of the CorTES were measured as a function of the bias voltage. Both noise spectra and the rms current noise between 100 and 20 kHz were determined. The intrinsic thermal time constant of the CorTES with heat capacity C and thermal conductance to the bath of G, $\tau_0 = C/G$, was determined from pulse response to be about 1.2 ms. Thus, the rms measurements are mainly sensitive to noise which is not suppressed by the electrothermal feedback [frequencies above $(2\pi\tau_0)^{-1} = 130$ Hz]. This method allows us to investigate the current noise against the operating point. When biased in the operating region ($V \lesssim 1$ μV), the noise in the CorTES cannot be accounted for by assuming contributions from TFN, JN, and SN, as can be seen in Fig. 3. We argue that the discrepancy cannot be explained by including an internal TFN (ITFN) [9,10] arising from the finite internal thermal impedance of the TES film. The ITFN is calculated as in Ref. [9] and it is proportional to $I\alpha$ exhibiting a peak at a bias corresponding to the maximum value of α. However, the ITFN does not explain the noise at lower bias voltages where the noise is more than a decade larger than what we would be expect just by assuming contributions from the previously known terms.

According to the Ginzburg-Landau theory, the free energy difference between equilibrium superconducting and normal states of a volume Ω in the absence of any fields is $F = \Omega(\alpha|\psi|^2 + 1/2\beta|\psi|^4)$, where $\alpha = 1.36\hbar^2/(4m\xi_0 l)(T/T_c - 1) \equiv \alpha_0(T/T_c - 1)$ and $\beta = 0.108/N(0)[\alpha_0/(k_B T_c)]^2$. Here m is the electron mass, and $N(0) = 1.33 \times 10^{34}$ cm^{-3} eV^{-1} is the density of states at Fermi level for Ti, $\xi_0 \approx 20$ μm is the BCS coherence length and $l \approx 100$ Å is the mean free path determined from the normal state resistivity. The temperature gradient within the normal section can be solved by $-\nabla(\kappa_N \nabla T) = j(r)^2\rho_n = V^2 L^{-1}[r\ln(r_b/r_0)]^{-2}$ using boundary conditions $T(r_b) = T_c$ and $\nabla T(r_0) = 0$. Fluctuations of ψ with free energy variations $\delta F \lesssim k_B T$ are possible and they correspond to large fluctuating volumes $\delta\Omega$ of the condensate near T_c. The temperature gradient restricts the fluctuations to an annular volume at the outer perimeter of the normal state part, where the coherence length $\xi(T) = 0.86\sqrt{\xi_0 l}/\sqrt{T/T_c - 1}$ diverges. We estimate the radial extent of fluctuations, δr, assuming that order parameter fluctuates between zero and its equilibrium value at a distance δr away from the equilibrium phase boundary within a volume $\delta\Omega = 2\pi r_b t \delta r$:

$$k_B T_c \simeq \delta F \simeq -\frac{\langle\alpha^2\rangle}{2\beta}\delta\Omega \simeq \frac{\pi\alpha_0^2 t\gamma^2 r_b}{\beta}\delta r^3. \qquad (1)$$

Here we have assumed that $(T/T_c - 1)$ can be approximated by $\delta r\gamma$, where γT_c represents the effective radial temperature gradient at the phase boundary. The solution for the temperature profile yields $\gamma = -V^2/[T_c^2 a L r_b \ln(r_b/r_0)]$, where the numerical factor $0 \le a \le 1$ is used as the only fitting parameter which describes the reduction of the Lorentz number close to the boundary due to the presence of Cooper pairs. Solving for δr and inserting the equations for α_0 and β, the fluctuation in boundary radius is given by $\delta r = 0.48[\pi N(0) k_B T_c r_b t\gamma^2]^{-1/3}$.

In order to obtain the spectral density of the critical fluctuations, we note that the relaxation time of a fluctuation is given by $\tau_{GL} = \hbar\pi[8k_B(T - T_c)]^{-1} = \hbar\pi[8k_B T_c\gamma\delta r]^{-1}$. For typical values of $\gamma\delta r$, 10 ns $< \tau_{GL} <$ 100 ns. Thus, the equivalent noise bandwidth is $\int_0^\infty (1 + \omega^2\tau_{GL}^2)^{-1} d\omega = \pi/(2\tau_{GL})$, and the resulting spectral density of the resistance fluctuations is given by $\delta R = \rho_n \delta r (2\pi t r_b)^{-1}\sqrt{2\tau_{GL}/\pi}$. This can be considered as a white noise source within the bandwidth of our measurement. The current noise arising from resistance fluctuations is given by $\delta I = dI/dR\ \delta R = I/(2R)(b + 1)\delta R$ where $R = V/I$ and $b = (R - R_s)/(R + R_s)$ corrects for nonideal voltage bias. The resistance fluctuations are suppressed by the ETF in a similar fashion as JN. More explicitly, the fluctuation superconductivity noise (FSN) component is given by

$$\delta I_{\mathrm{FSN}}(\omega) = \frac{I\delta R}{R}\frac{1 + b}{2(1 + bL_0)}\frac{\sqrt{1 + \omega^2\tau_0^2}}{\sqrt{1 + \omega^2\tau_{\mathrm{eff}}^2}}, \qquad (2)$$

where $bL_0 = VI\alpha/(GT)$ is the loop gain of the negative electrothermal feedback, and $\tau_{\mathrm{eff}} = \tau_0/(1 + bL_0)$ is the

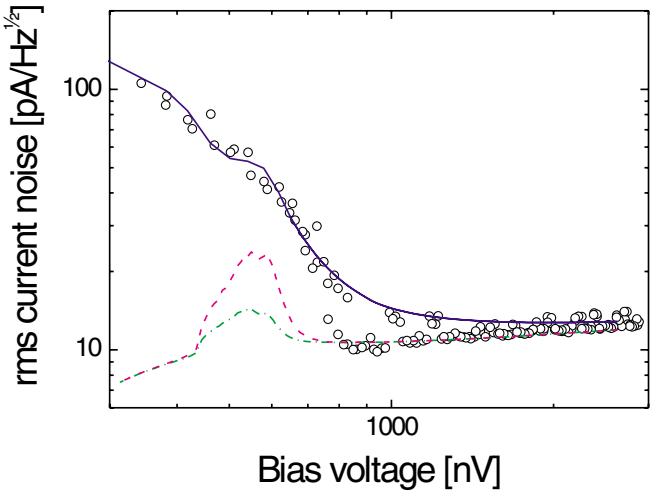

FIG. 3 (color online). The average rms current noise in a frequency band from 100 to 20 kHz (marked by open circles) measured at a bath temperature of 20 mK. The total modeled noise is the solid line, and it consists of TFN, JN, SN, ITFN, and fluctuation superconductivity noise (FSN). The dash-dotted line represents a model with only TFN, JN, and SN included. The dashed line represents a model with TFN, JN, SN, and ITFN.

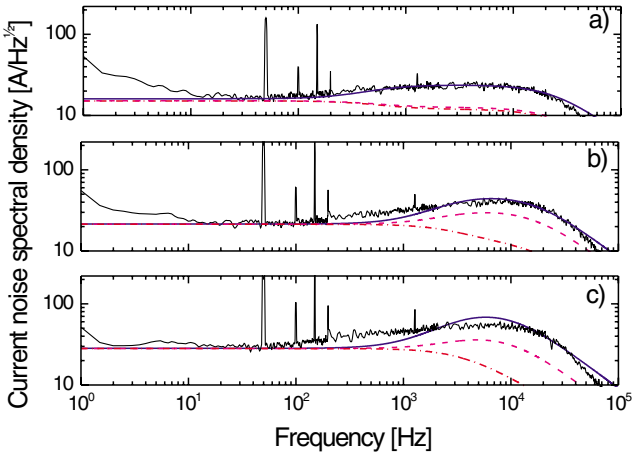

FIG. 4 (color online). Noise spectra measured at a bath temperature of 20 mK at bias voltages of (a) 0.75 μV, (b) 0.62 μV, and (c) 0.5 μV. The notation for the different modeled noise components is identical to that of Fig. 3.

effective time constant of the sensor. As Figs. 3 and 4 show, the noise can be accurately modeled throughout the transition and over a wide range in frequency with only one fit parameter, $a = 0.1$. We should, however, keep in mind that the crude definition of δr in our model may simply be compensated by this fitting parameter.

When FSN dominates over the other noise terms, the FWHM energy resolution of a calorimeter can be estimated from the noise equivalent power $\mathrm{NEP}_{\mathrm{FSN}} = \delta I_{\mathrm{FSN}}/S_I$ where S_I is the current responsivity of the sensor [11],

$$\Delta E \approx 1.18\left[\int_0^\infty \frac{df}{\mathrm{NEP}_{\mathrm{FSN}}{}^2(f)}\right]^{-1/2} = 1.18\frac{VI}{L_0 R}\delta R\sqrt{\frac{2\tau_0}{\pi}} = 1.18 I^2 \frac{\delta R}{L_0}\sqrt{\frac{2\tau_0}{\pi}}. \quad (3)$$

In the measured device, ΔE_{FSN} has a minimum value of $\sim$0.1 eV at $V = 0.55$ μV (where α is at maximum) and it increases to 29 eV at $V = 0.3$ μV. This implies that the energy resolution of TES microcalorimeters degrades significantly if biased at a voltage below that corresponding to maximum of α.

In summary, we have fabricated and analyzed an idealized transition-edge sensor in which edge effects are excluded. An analytical steady-state model has been developed which shows good agreement with the measured $I(V)$ curve. The CorTES is insensitive to external magnetic fields due to a current carrying Nb ground plane. As a result, the α remains above 300 even when biased with constant voltage bias. We show that the previously unexplained extra noise originates from thermal fluctuations of the phase boundary. The same noise mechanism is present in all types of superconducting transition-edge sensors [12], but the effect might not be observable in some cases depending on the way the phase boundaries configure themselves.

This work has been supported by the Academy of Finland under the Finnish Centre of Excellence Programme 2000-2005 (Project No. 44875, Nuclear and Condensed Matter Programme at JYFL), and by the Finnish ANTARES Space Research Programme under the *High Energy Astrophysics and Space Astronomy* (HESA) consortium. The work of HFCH and WBT is financially supported by the Dutch Organisation for Scientific Research (NWO). The authors gratefully acknowledge K. Hansen, N. Kopnin, and H. Seppä for their comments.

[1] K. D. Irwin, G. C. Hilton, D. A. Wollman, and J. M. Martinis, Appl. Phys. Lett. **69**, 1945 (1996).
[2] W. B. Tiest *et al.*, in *Low Temperature Detectors 9 (LTD-9)*, edited by F. S. Porter, D. McCammon, M. Galeazzi, and C. Stahle, AIP Conf. Proc. No. 605 (AIP, New York, 2002), pp. 199–202.
[3] A. Luukanen *et al.*, *Summary Report, European Space Agency*, ESA Contract No. 12835/98/NL/SB, ESA-ESTEC, ADM-A, Keplerlaan 1, NL-2200 AG Noordwijk.
[4] G. C. Hilton *et al.*, IEEE Trans. Appl. Supercond. **11**, 739 (2001).
[5] A. Luukanen and J. P. Pekola, Appl. Phys. Lett. **82**, 3970 (2003).
[6] D. W. Floet, E. Miedema, and T. Klapwijk, Appl. Phys. Lett. **74**, 433 (1999).
[7] R. Berman, in *Thermal Conduction in Solids* (Oxford University Press, Oxford, 1976), Chap. 12, pp. 164–168.
[8] M. M. Leivo and J. P. Pekola, Appl. Phys. Lett. **72**, 1305 (1998).
[9] H. F. C. Hoevers *et al.*, Appl. Phys. Lett. **77** 4422 (2000).
[10] J. M. Gildemeister, A. T. Lee, and P. L. Richards, Appl. Opt. **40**, 6229 (2001).
[11] D. M. S. H. Moseley and J. C. Mather, J. Appl. Phys. **56**, 1257 (1984).
[12] K. E. Nagaev, Physica (Amsterdam) **184C**, 149 (1991).